Received: 22 July 2021 | Revised: 25 January 2022 | Accepted: 25 February 2022

DOI: 10.1002/eqe.3638

RESEARCH ARTICLE

WILEY

On the seismic loss estimation of integrated performance-based designed buildings

Davit Shahnazaryan | **Gerard J. O'Reilly** | **Ricardo Monteiro**

Centre for Training and Research on Reduction of Seismic Risk (ROSE Centre), Scuola Universitaria Superiore IUSS di Pavia, Italy

Correspondence
Gerard J. O'Reilly, Centre for Training and Research on Reduction of Seismic Risk (ROSE Centre), Scuola Universitaria Superiore Pavia, Piazza della Vittoria n. 15, Pavia, IT 27100, Italy.
Email: gerard.oreilly@iusspavia.it

Funding information
Italian Ministry of Education, University and Research

Abstract

Performance-based earthquake engineering (PBEE) is a probabilistic framework developed to improve seismic risk decision-making, characterising building performance in terms of metrics such as casualties, economic losses and anticipated downtime. Building upon PBEE, expected annual loss (EAL) and collapse safety expressed in terms of mean annual frequency of collapse (MAFC) have been recently proposed as fundamental objectives within an integrated performance-based seismic design (IPBSD) framework. This article, following the parametric investigations conducted, proposes a refined design loss curve and demonstrates the capabilities of IPBSD to target a certain MAFC and limit EAL through its application to several reinforced concrete case-study buildings. The performance was evaluated using both incremental dynamic analysis and a storey-based loss assessment procedure to estimate MAFC and EAL of risk-targeted designs, respectively. The agreement and consistency of design solutions and intended performance objectives were then checked to demonstrate the validity of the IPBSD framework, with MAFC being effectively targeted and the EAL limited as initially foreseen by the method. Further scrutiny of the results highlighted the validity of the assumptions made in the IPBSD framework and shed further light on the pertinent sources of economic losses, namely the ones deriving from structural and non-structural elements, when designing buildings, in addition to influential parameters like initial period range and the influence of design engineering demand parameter profiles. This is seen as part of the next-generation risk-targeted and loss-driven design approaches in line with modern PBEE requirements.

KEYWORDS

expected annual loss, mean annual frequency of collapse, PBEE, reinforced concrete, risk-targeted design

1 | INTRODUCTION

The protection of human lives has been a primary goal of traditional seismic design guidelines, requiring the limitation of structural collapse through sufficient strength and ductility provisions, in addition to proper member detailing. Also, a controlled and stable ductile mechanism during strong earthquakes should be ensured through the so-called

capacity design. Neglecting damage at more frequent events during the design stage may have severe consequences during an earthquake, as damage to structural and especially non-structural elements may result in disproportionally high economic losses. Therefore, to ensure an overall satisfactory building performance, performance-based earthquake engineering (PBEE) was introduced during the 1990s with the Vision 2000 framework[1] to relate predefined states of damage to certain levels of ground shaking. Based on the initial interpretations of PBEE, a more probabilistic framework was developed, which became known as the Pacific Earthquake Engineering Research (PEER) Center PBEE methodology.[2] It quantifies the mean annual frequency of exceedance (MAFE) of a limit state (LS), through the integration of the probability of reaching such an LS for a chosen intensity measure (IM) with its site hazard curve.[3] PBEE quantifies the performance of a given structural system by using a fully probabilistic framework and analysis tools with a solid scientific basis to improve seismic risk decision-making and express the levels of performance in terms of metrics meaningful to stakeholders and building owners (e.g., casualties, economic losses or anticipated downtime). Due to its probabilistic nature and computationally expensive implementation, the framework has been primarily employed within academic or specialised research[4,5] rather than widespread implementation among practitioners. Moreover, given the nature of the framework, it has been primarily developed for the assessment of existing buildings rather than the design of new ones.

With the above considerations in mind, this article builds on and further validates a framework recently proposed by Shahnazaryan and O'Reilly[6] to explore the impacts of design decisions on the effective limitation of losses. The framework uses collapse risk and economic loss as main design inputs, while the performance objectives remain in line with the goals of PBEE.[7] The proposed framework is extended to 3D buildings with the consideration of damageable component inventory sensitive to the seismic action in both directions. Additionally, a Python-based iterative object-oriented toolbox was developed to aid practitioners carry out a seamless loss-driven risk-targeted design. The framework is briefly recalled and described through an application to buildings with reinforced concrete (RC) moment-resisting frames (MRF) as the main lateral load resisting system. Then, the ability of the framework in satisfying the pre-established performance objectives (i.e., limitation of economic loss while maintaining collapse safety) is validated through its application to several case-study buildings. A detailed dissection of the main sources of losses within the structures is examined to shed further light and provide justification needed for the simplifying assumptions, made as part of such a framework, initially outlined by O'Reilly and Calvi.[8] Furthermore, the proposed IPBSD framework is also compared with the response of buildings designed according to conventional seismic codes, such as Eurocode 8.[9]

2 | INTEGRATED PERFORMANCE-BASED SEISMIC DESIGN (IPBSD)

2.1 | Performance objectives

As mentioned above, the primary focus of modern seismic design codes is to provide life safety to building occupants by avoiding structural collapse. With this primary objective addressed, the performance during frequent seismic events is checked and verified. Implemented at return periods of 475 and 95 years, these are termed as the *no-collapse* and *damage limitation requirements* in the current version of Eurocode 8 (EC8), with the possibility to account for building importance class. Similarly, *serviceability* and *ultimate* limit states associated with design return periods of 25 and 500 years, respectively, are defined in New Zealand's NZS1170,[10] with the possibility of modifications via importance classes. With slight modifications, a revised design code in the US, ASCE7-16,[11] sets a fraction of the maximum considered event for the design of the building, determined from a series of risk-targeted hazard maps developed for a target collapse risk of 1% in 50 years.

Those seismic design codes follow a force-based design (FBD) method, which calculates a design base shear force from a reduced elastic spectrum using either the equivalent lateral force method or response spectrum method of analysis. Priestley[12] and others pointed out several shortcomings regarding the FBD method, thus advocating a displacement-based design (DBD) approach, where deformation demands in the individual elements drive the design process, resulting in the development of the direct displacement-based design (DDBD) method[13] and other similar methods.[14] While both FBD and DDBD are good approximations for the initial seismic design of structures, neither explicitly quantifies the structural performance in a way that may be considered as fully satisfying the goals and needs of modern PBEE. Essentially, this means that the performance of structures designed using either method will not be considered as risk-consistent (i.e., the annual probability of exceeding a certain performance threshold is not accurately known or consistent among different structures), and metrics such as building collapse risk, expected economic losses or downtime are not included in the design process. Therefore, a more risk-targeted and probabilistic framework has been sought in recent years.

Integrated performance-based seismic design (IPBSD) was proposed as a framework to evaluate building performance and identify structural solutions meeting the target collapse risk and limiting the economic loss. It was expanded from the conceptual seismic design framework developed by O'Reilly and Calvi,[8] which requires very little structural information at the design onset and has a goal of limiting the expected annual loss (EAL) of the building. It was further developed by Shahnazaryan and O'Reilly[6] to explicitly target collapse risk in terms of mean annual frequency of collapse (MAFC) along with the limitation of EAL. While they demonstrated the validity of the framework in identifying structural solutions for planar RC MRFs, which met the target MAFC set forth as the performance objective, this article aims to extend the IPBSD framework to three-dimensional (3D) buildings. Furthermore, and perhaps more crucially, it also provides further insight and validation for the initial assumptions made to meet both the target MAFC and EAL limits for bidirectional behaviour, the latter of which is yet to be tested and verified in detail.

Several assumptions are made to relate the performance objectives to a design solution space, which is now pertinent to both principal directions of the building. The target MAFC, $\lambda_{c,target}$, is used to limit the actual λ_c described by Equation (1):

$$\lambda_c = \int_0^{+\infty} P\left[C|Sa\left(T_1\right)\right] \left|dH\left(Sa\left(T_1\right)\right)\right| \leq \lambda_{c,target} \tag{1}$$

where $Sa(T_1)$ is the IM and is defined as the spectral acceleration at fundamental period, T_1, $P[C|\, Sa(T_1)]$ is the probability of collapse given the IM level, and $H(Sa(T_1))$ is the site hazard curve expressing the mean annual frequency of exceeding a given IM level. An EAL limit, $\lambda_{y,limit}$, is used to control the EAL, λ_y, described by Equation (2) such that excessive losses do not manifest over the lifetime of the building.

$$\lambda_y = \int_0^{+\infty} E\left[y\right] \left|dH\left(Sa\left(T_1\right)\right)\right| \leq \lambda_{y,limit} \tag{2}$$

where $E[y]$ is the expected loss characterised obtained from the loss curve detailed further below.

2.2 | IPBSD implementation

An overview of the IPBSD framework implementation is briefly outlined with the flowchart depicted in Figure 1, whereas a detailed description can be found in Shahnazaryan and O'Reilly.[6] Particular emphasis is given to the developments and refinements made in this study, supported by parametric studies presented in later sections.

2.2.1 | Preliminary building information and design loss curve

Before initiating IPBSD, some preliminary building information is needed along with the definition of site hazard (Figure 1, Step 1a), namely material properties, global dimensions, lateral load resisting system configuration, gravity loads, and replacement cost of the building.

At the beginning of IPBSD, a suitable loss curve is identified to limit λ_y. Performance limit states are characterised through the expected loss ratio (ELR), y, and MAFE, λ, as shown in Figure 2. The loss curve uses three limit states: fully operational limit state (OLS), which defines the onset of damage and monetary loss, assumed to have $y_{OLS} = 1\%$ and associated with a return period of 10 years; serviceability limit state (SLS), where the economic losses are controlled through the modification of y_{SLS}; and collapse limit state (CLS), where complete collapse (i.e., $\lambda_{CLS} = \lambda_c$) and economic loss of the building (i.e., $y_{CLS} = 100\%$) are expected. The area under the loss curve is the design EAL, λ_y and the characteristics associated with SLS should be adjusted to make sure that λ_y does not exceed $\lambda_{y,limit}$, ensured by the selection of λ_{SLS} in line with seismic code requirements. If the limit is exceeded, the limit state parameters need to be adjusted and the loss curve must be recomputed (Figure 1, Step 1b).

In order to ensure that losses are not excessive, a building should be designed to accommodate y_{SLS}, whereby the loss contributions from peak storey drift (PSD) and peak floor acceleration (PFA)-sensitive components are limited, leading to the identification of a range of possible initial (i.e., secant to yield) structural periods $[T_{lower}, T_{upper}]$ for each prin-

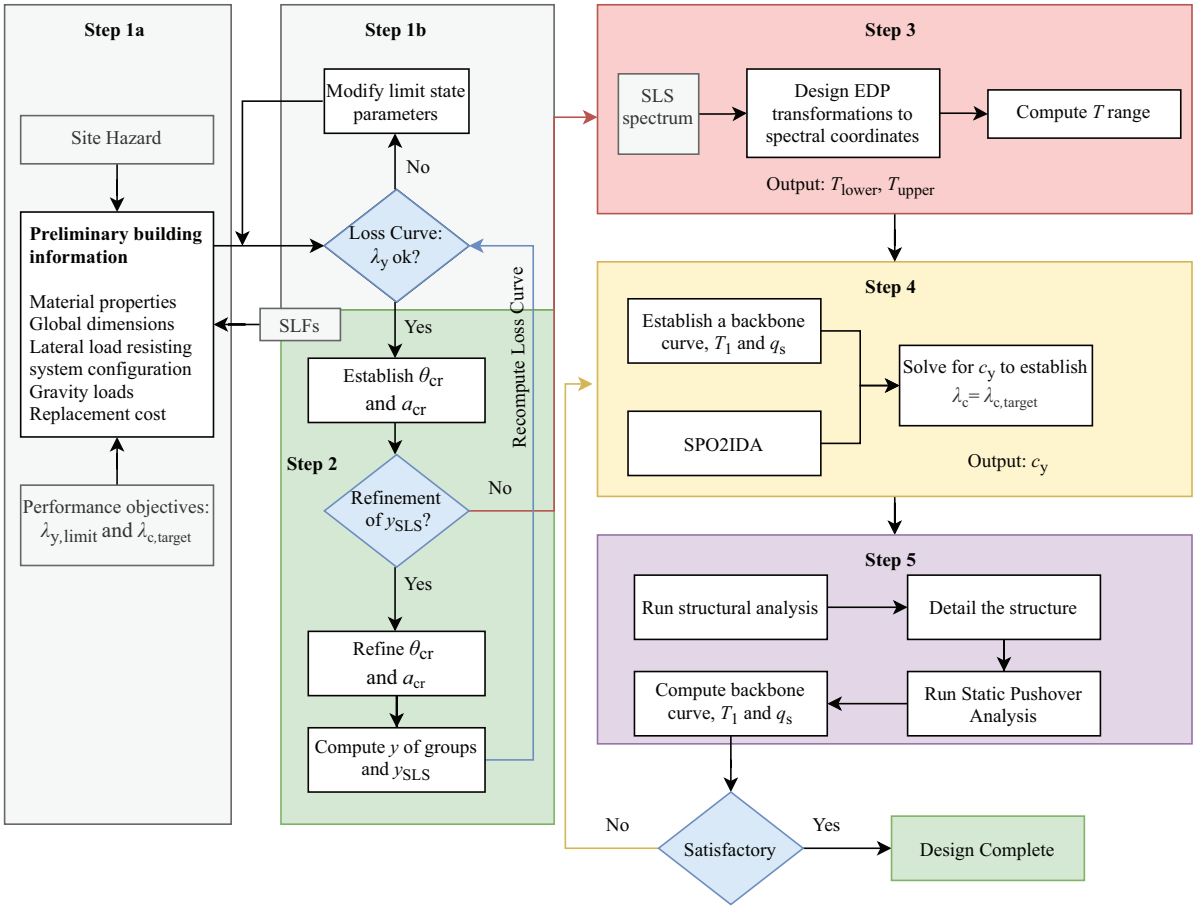

FIGURE 1 Flowchart of the IPBSD framework

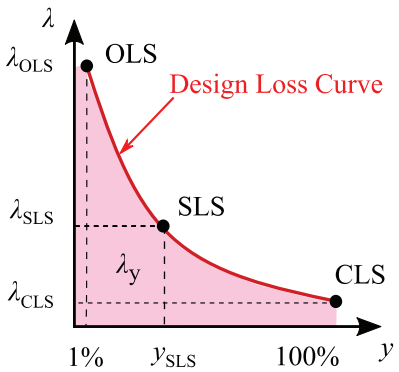

FIGURE 2 Identification of the loss curve and SLS performance objectives to limit the EAL

cipal direction of the building. The IPBSD framework is independently applied in each direction sequentially, without disturbing the integrity of results in the perpendicular direction (e.g., design and detailing of corner columns must be the same or static or pushover analysis should be applied to a 3D building model). Before embarking on the computation of a feasible period range, storey loss functions (SLFs) relating structural demands and economic losses need to be selected or generated, which can be facilitated through a tool recently proposed by Shahnazaryan et al.[15] Decisions should be made with regard to subdividing components into different damageable performance groups: structural PSD-sensitive; non-structural PSD-sensitive; and non-structural PFA-sensitive. SLFs should be developed for each storey level and each damageable group. Once the SLFs are generated or selected, relative weights or contributions of different damageable

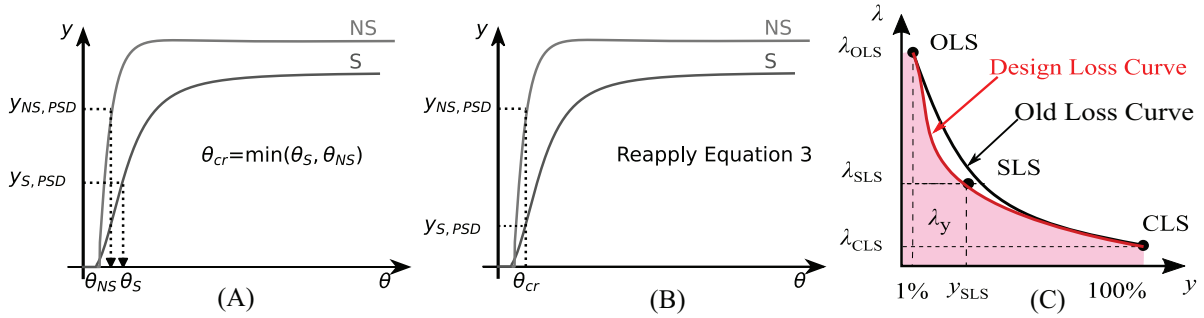

FIGURE 3 Storey loss functions and computation of design limits (S and NS denote structural and non-structural component groups, respectively). (A) Computation of θ_{cr} and identification of θ for non-structural (NS) and structural (S) components; (B) Reapplication of Equation (3) and estimation of $y_{NS,PSD}$ and $y_{S,PSD}$; (C) Computation of design loss curve

groups to expected loss, Y, at SLS are defined. The ELR at SLS, y_{SLS}, shown in Figure 2 is broken down as per Equation (3).

$$y_{SLS} = \sum_{1}^{i} \left(y_{i,S,PSD} + y_{i,NS,PSD} \right) + \sum_{0}^{j} y_{j,NS,PFA} \tag{3}$$

where $y_{i,S,PSD}$ is associated with structural PSD-sensitive, $y_{i,NS,PSD}$ is associated with non-structural PSD-sensitive, and $y_{i,NS,PFA}$ is associated with non-structural PFA-sensitive loss contributions, i is the number of storeys, j is the number of floors and 0 refers to the ground floor where non-structural PFA-sensitive losses are also present. Additionally, each of the PSD contributions comprises damageable components sensitive to the direction of the seismic action (i.e., the principal directions of the building), while, generally, PFA-sensitive components are considered sensitive to both directions and a non-directional factor is applied to account for the increased demands and therefore associated losses on the components. The loss contributions for each building level and, in the case of components with directionality properties, along each direction of the building, may be computed as the product of target y_{SLS} and its relative weighting Y by Equation (4). The Y weighting factors depend on the component inventory information and therefore on the SLFs developed.

$$\begin{aligned} y_{S,PSD} &= y_{SLS} Y_{S,PSD} \\ y_{NS,PSD} &= y_{SLS} Y_{NS,PSD} \\ y_{NS,PFA} &= y_{SLS} Y_{NS,PFA} \end{aligned} \tag{4}$$

2.2.2 | Refinement of design loss curve

Having computed all possible ELR values at the different storey or floor levels, as well as directions of the building, demand limits in terms of critical PSD, θ_{cr}, and maximum PFA, a_{cr}, may be computed using the SLFs shown in Figure 3 for each direction. The computation process is applied to each principal direction of the building considering damageable groups only sensitive to the direction of interest and all non-directional damageable groups with the application of a non-directional factor. Satisfying these conditions, in both directions, is expected to result in the fulfilment of the EAL limit initially set out, as described by Shahnazaryan and O'Reilly[6] and will be validated numerically here in Section 5. Therefore, two separate design limits are obtained associated with each direction. By entering the vertical axis in Figure 3A with the values computed via Equation (4), the more critical (lower) θ_{cr} and a_{cr} are obtained (an example flow of the computation is given for PSD sensitive components considering two fictitious SLFs). However, this entails the use of the same θ_{cr} for both structural and non-structural components (θ_S and θ_{NS}, respectively, in Figure 3). In other words, if θ_{cr} was associated with non-structural components (i.e., more vulnerable components), then the assumed value of $y_{S,PSD}$ for the structural elements estimated via Equation (4) is likely to be overestimated while the actual value of $y_{S,PSD}$ associated with θ_{cr} will be lower, as shown in Figure 3B. Here, $y_{S,PSD}$ is considerably lower than what was hypothesised earlier in Equation (4). Therefore, to avoid the possible underestimation of $\lambda_{y,limit}$, which would be the case following the initial assumptions proposed by O'Reilly and Calvi,[8] a proposed single-step refinement through the reapplication of Equation (3) is presented in this work (Figure 1, Step 2), using the modified ELRs of damageable groups (i.e., the newly computed significantly

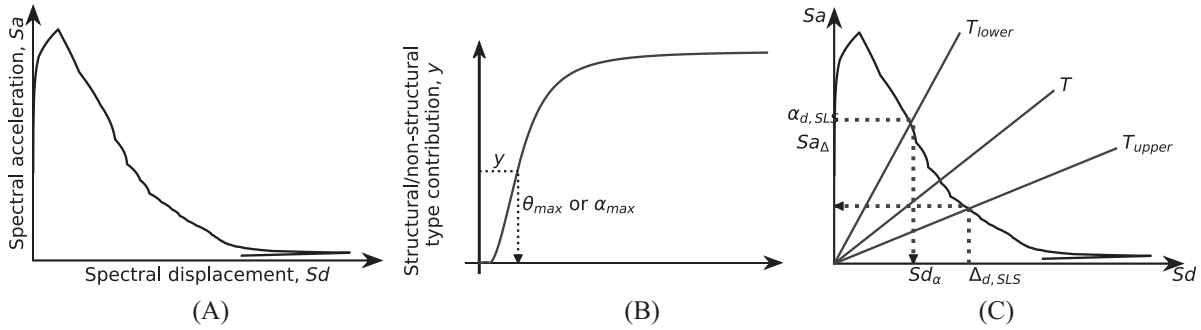

FIGURE 4 Establishment of a feasible initial period range. (A) Design spectrum at SLS, (B) SLF and estimation of design limits, (C) identification of period limits

lower $y_{S,PSD}$), where applicable. The refinement step is not mandatory to the IPBSD framework but should be applied if more refined or less conservative results are sought. If the refinement step is not undertaken, the design moves on to Step 3 in Figure 1. Otherwise, as a result of the refinement, the new value of y_{SLS} will be lower, thus resulting in a loss curve that is shifted to the left as shown in Figure 3C, which will also be observed later in Section 6 through actual results from numerical analysis.

This step proposed here acts as a single-step iteration where the framework, due to the dissimilarity of component fragilities and costs associated with different damageable groups, tries to adjust the assumptions made before the initiation of further computations for the optimization of the solution space towards values desirable by the practitioner. This will provide consistency for loss contribution computation associated with more robust components. Based on the refined y_{SLS}, the loss curve is updated as shown in Figure 3C and a new design EAL, which is lower than the initial value, is identified and compared against the limit $\lambda_{y,limit}$. Alternatively, the practitioner may modify the y_{SLS} to take advantage of this initial conservatism and refine λ_y to be in the vicinity of $\lambda_{y,limit}$ defined before the onset of the framework. The developments discussed herein will be further detailed and assessed through exploratory analyses in Section 6.

2.2.3 | Identification of initial period range

Next, the design spectrum at SLS (Figure 4A) and SLFs (Figure 4B) are used to compute the structural demand limits, which, in combination with the design spectrum, may be used to identify the range bounded by the lower, T_{lower} and upper, T_{upper} period limits, as demonstrated in Figure 4C and Step 3 of Figure 1. The building should essentially have secant to yield periods within these ranges in both directions, ensuring that it will be neither too stiff, which would result in excessive floor acceleration-sensitive losses, nor too flexible, which would result in excessive drift-sensitive losses, at SLS. Satisfying these conditions in both directions is expected to result in fulfilment of the EAL limit initially set out, as will be confirmed in the analysis in Section 6.

2.2.4 | Controlling structural collapse

With economic loss limited by ensuring that periods along each direction of the building are within the respective period ranges, it is important to control the risk of structural collapse (Figure 1, Step 4). A period between T_{lower} and T_{upper} is selected and the expected backbone behaviour and overstrength, q_s, are first trialled by the practitioner (Figure 5(left)). Here, q_s represents the ratio between the strength at yield, V_y, and design, V_d, and q_μ is the ratio between spectral acceleration at collapse, Sa_c, and yield, Sa_y, while Δ_y, Δ_c and Δ_f represent displacements at yield, capping and fracturing points, respectively. The SPO2IDA tool[16] is used to estimate the collapse fragility function of the building along each direction in terms of median collapse capacity, Sa_c, and record-to-record (RTR) variability, β_{RTR}, assuming a lognormal distribution. Throughout the IPBSD procedure implemented here, only RTR variability has been considered for simplicity, although other pertinent sources do exist (e.g., modelling uncertainty[17]) but may be easily considered in the process. For example, the uncertainty value β_{RTR} obtained from SPO2IDA may be amplified via a square root sum of the squares (SRSS) approach to consider other independent sources of response uncertainty in the collapse capacity estimation. Further-

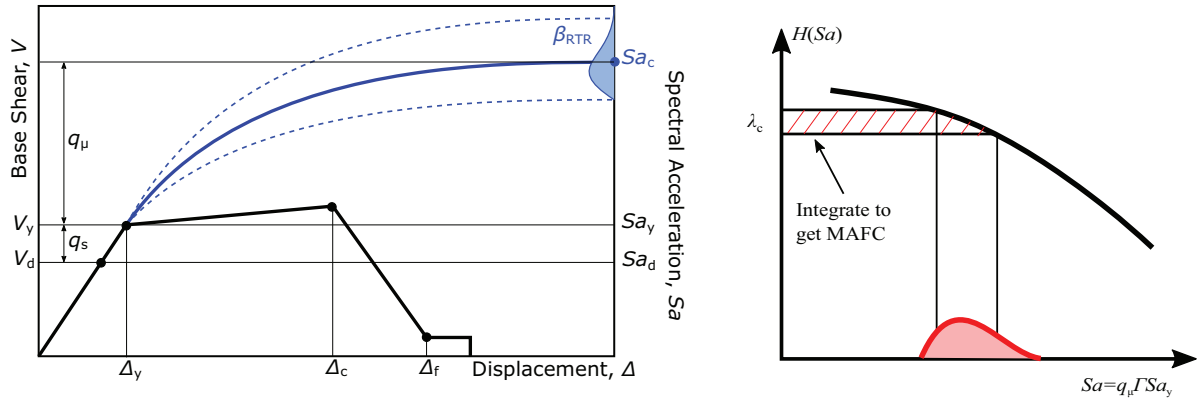

FIGURE 5 (left) Expected backbone behaviour and (right) Identification of collapse capacity and computation of λ_c

more, the additional uncertainty in the non-collapse response may be considered at SLS. That is, during Phase 2 of the IPBSD description in Shahnazaryan and O'Reilly,[6] the inherent uncertainty at SLS, β_{SLS}, in Equation (7) in that publication may also be amplified via SRSS to account for these additional sources of uncertainty. Having assumed the static pushover (SPO) shape (backbone curve), the SPO2IDA tool may be used to perform a quick estimation of the dynamic response and capacity. The output of SPO2IDA is the collapse fragility function, which is then integrated with the hazard curve corresponding to the selected T_1, $H(Sa(T_1))$, to compute λ_c (Figure 5(right)). The trialled structural capacity of the frame, q_s and/or backbone shape characteristics are revised until λ_c equates to $\lambda_{c,target}$, satisfying Equation (1). The process is repeated for each principal direction of the building and the critical (larger) of Sa_y is selected as the design yield strength for further design and detailing.

2.2.5 | Design and detailing

The identified design base shear is then used to compute the lateral distribution of forces and perform static analysis including gravity loads to estimate demands on structural elements. Seismic design codes may be followed to perform member detailing to determine the required element cross-section dimensions and reinforcement content. Strength hierarchy and local ductility requirements must be accounted for as well. The final structural solutions should have T_1 in both directions within a reasonable tolerance of the assumed value and within the feasible period range identified. If the condition is met, the identified structural configuration may be adopted. Otherwise, the element dimensions and reinforcement content should be revised (Figure 1, Step 5).

2.3 | Python-based iterative framework

To aid the designer in some of the cumbersome tasks involved within the framework, specifically regarding the assumption of the backbone curve shape or computation of design yield strength, an object-oriented Python-based software has been created and is freely available on GitHub.[18] The software is based on the framework described here and in previous works by the authors. Some of the more tedious aspects involving iterations or calibrations are automated within the software to simplify the tasks for a designer. However, it is noted that the use of this software is not a strict requirement to implement IPBSD but rather a supplementary tool to facilitate and expedite the process for users familiar with the design steps. The open-source and object-oriented nature of the code lets users customise and tailor their code to suit diverse design situations.

Essentially, based on the design Sa_y, lateral force analysis including the gravity loads is carried out for both directions of the building and the structural elements are designed following the recommendations of Eurocode 2, EC2[19] and EC8. Based on the maximum demands from both analyses, structural elements are designed using moment-curvature relationships attained following the Response-2000 sectional analysis program,[20] which utilises the concrete and reinforcement material properties of EC2. The output will be the hysteretic hinge model properties or the spring properties based on the recommendations of Haselton et al.,[21] depending on the choice of the hinge model types. Hinge properties are then

TABLE 1 Case-study building configurations

Case	Seismicity	Configuration			$\lambda_{c,target}$	$\lambda_{y,limit}$ (%)
		N_{st}	N_x	N_y		
1-IPBSD	High	2	4	3	2.0×10^{-4}	0.60
2-IPBSD	High	2	4	3	2.0×10^{-4}	0.80
3-IPBSD	High	2	4	3	1.0×10^{-4}	0.60
4-IPBSD	High	4	4	3	2.0×10^{-4}	0.60
5-IPBSD	High	4	4	3	2.0×10^{-4}	0.80
6-IPBSD	High	4	4	3	1.0×10^{-4}	0.60
7-IPBSD	High	6	4	3	2.0×10^{-4}	0.60
8-IPBSD	High	6	4	3	2.0×10^{-4}	0.80
9-IPBSD	High	6	4	3	1.0×10^{-4}	0.60
10-IPBSD	Medium	2	4	3	2.0×10^{-4}	0.60
11-IPBSD	Medium	4	4	3	2.0×10^{-4}	0.60
12-IPBSD	Medium	6	4	3	2.0×10^{-4}	0.60

fed into the module, which, using OpenSees,[22] creates a 3D numerical model of the building and runs a modal analysis to compute the modal properties of the building. Rayleigh damping with 5% of critical damping assigned to the principal modes associated with the directions of the building is used, although other damping models may be used[23] but the impact of this choice is not pursued further here. Then, SPO analysis is carried out to calculate the backbone curve in both directions. Based on the findings, a new estimate of the backbone curve shape, as well as secant-to-yield periods, are used to calibrate the input arguments for the SPO2IDA toolbox. These iterations are automated and are repeated until convergence of assumptions is achieved and the final solution is derived. It is again important to note that, due to the modularity of the software, different building code recommendations, as well as different procedures for the detailing of structural elements, may be adapted.

3 | CASE-STUDY APPLICATION

3.1 | Definition of case-study buildings and numerical modelling

Several case-study buildings were defined and the IPBSD framework was applied. Similarly, EC8 provisions were applied to design buildings of similar configurations. With the solutions identified, non-linear numerical models were produced, and incremental dynamic analysis (IDA) was performed, followed by loss assessment to numerically verify the validity of different design methods and compare them with the loss-driven risk-targeting framework outlined earlier. Twelve case-study buildings consisting of RC MRFs in a *space* configuration were examined and are described in Table 1. The designs vary in terms of the number of storeys, design targets in terms of MAFC and EAL, as well as seismicity region. Two seismic locations in Italy were selected corresponding to soil type C, as defined by EC8, with L'Aquila representing high seismicity and Ancona representing medium seismicity. In Table 1, the case number reflects the unique identifier for each case-study building, N_{st} is the number of storeys, N_x and N_y are the number of bays in X (first principal direction) and Y (second principal direction). Ground and typical storey heights are 3.5 and 3.0 m, respectively, while the bay widths in both directions are 4.5 m.

The value of $\lambda_{y,limit}$ was indicatively selected considering designs code-compliant with a rating of "A" or higher, according to the classification proposed by Cosenza et al.[24] thus with values lower than 1%. In addition, Ramirez et al.[25] and Goulet et al.[26] have found values from 0.6% to 1.1% for RC MRF spatial buildings designed according to the design and seismic provisions in force at the time in the US. Keeping this in mind, two different limits of 0.6% and 0.8% were selected to explore the variation of design solutions. Regarding $\lambda_{c,target}$, various values are reported in the literature and discussed in Shahnazaryan and O'Reilly.[6] For example, ASCE 7–16[11] recommends an acceptable national risk of 1% in 50 years (2.0×10^{-4}), while other studies from the literature suggest values of around 1.0×10^{-5}.[26–28] Additionally, Dolšek et al.[29] noted typical limits between 10^{-4} and 10^{-5}, while Silva et al.[30] used 5.0×10^{-5} when discussing the development of risk-targeted hazard maps for Europe. Accordingly, a decision was made to select two different values of 2.0×10^{-4} and

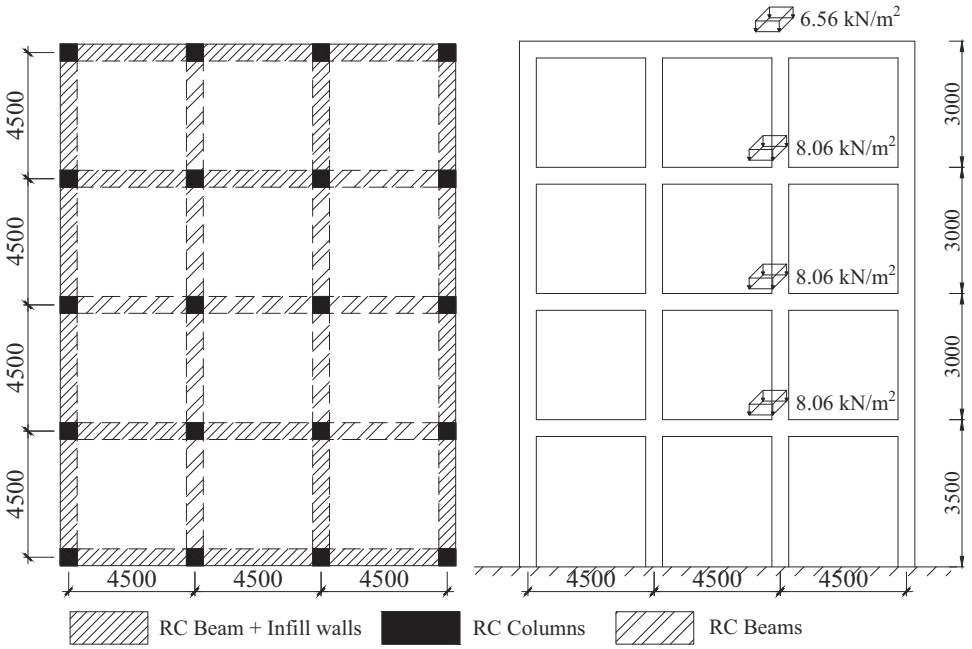

FIGURE 6 Illustration of (left) plan layout and (right) elevation of the case-study buildings

1.0×10^{-4} for $\lambda_{c,target}$, also highlighting the capability of easily tailoring the design performance objectives within the IPBSD framework.

Typical plan and elevation layouts are shown in Figure 6. The gravity loads, including imposed and dead loads, were assumed as 8.06 kN/m^2 and 6.56 kN/m^2 at the typical floor and roof level, respectively. Dead loads included an assumption of a RC slab of 150 mm thickness and a partial safety factor of 1.35, while imposed loads assumed a Category A for residential buildings with a load of 2 kN/m^2 and a roof load of 1 kN/m^2 with a partial safety factor of 1.5, in line with EC2.[19] The specific weight of the concrete was taken as 25 kN/m^3. The material properties used in the design and detailing were 25 MPa for the concrete compressive strength and 415 MPa for the steel yield strength. No plan or elevation irregularities were considered.

The case-study buildings outlined were designed and examined following different methodologies. The IPBSD framework and the EC8's equivalent lateral force approach was implemented. The goal was to demonstrate the capability of having loss-driven risk-consistent designs following the IPBSD framework when compared to a code-based design formulation. The case-study buildings were detailed and sized following the EC8 and EC2 member detailing requirements.

For all case-study buildings, 3D numerical models were generated using OpenSees[22] to perform SPO and NLRHA. The masses were lumped at each floor and the nodes were constrained in the horizontal direction to mimic a rigid diaphragm behaviour. The concentrated plasticity approach developed by Ibarra et al.[31] was used to consider non-linear behaviour in beams and columns. The plastic hinges at both ends of beams and columns were modelled using a lumped plasticity model with bilinear hysteretic properties available in OpenSees, while the elastic sections of the elements were modelled using an elastic cracked section stiffness object. Concrete compressive strength was assumed 25 MPa while the yield strength of reinforcement was taken as 415 MPa. All columns were fixed at the base. Rayleigh damping was implemented with 5% of critical damping assigned to principal modes associated with each direction of the building. To obtain the hysteretic models, the backbone curve associated with each structural element was fit to the moment-curvature relationship of the element obtained using Response-2000. Additionally, the plastic hinge length required for the hysteretic model was computed following Priestley et al.[13] P-Delta effects were considered through application of vertical gravity loads during non-linear analysis and consideration of the P-Delta transformation method available in OpenSees. Beam-column joints were assumed to be rigid, and no shear mechanisms were modelled since the design of the structure followed capacity design criteria hence no shear failures are expected. It is important to note that torsional response of the building was not explored given the main scope of this study. Additionally, attempting to address situations where torsional response is pertinent may not be appropriate. In such cases, the IPBSD may be considered as a method useful for providing a more optimal initial design satisfying more advanced performance goals, but these design solutions would necessitate detailed analysis for their verification.

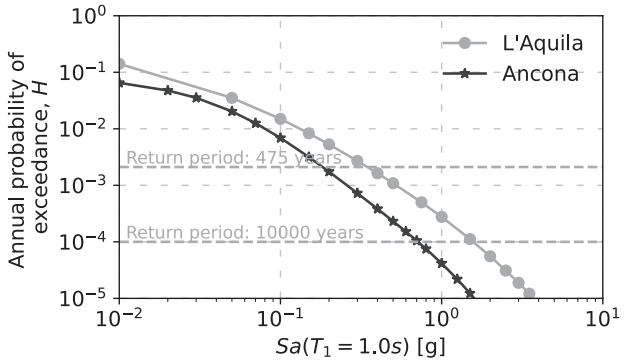

FIGURE 7 Seismic hazard for both sites analysed at a spectral acceleration at a period of $T_1 = 1.0$ s

3.2 | Site hazard and ground motions

Probabilistic seismic hazard assessment (PSHA) analyses were performed using OpenQuake[32] for the two site locations with the SHARE hazard model.[33] A set of 30 ground motion records (consisting of two horizontal components) were selected from the NGA West-2 database[34] with each record's soil type being consistent with that of the site. The ground motions were selected to be representative of the site without any specific selecting and scaling approach in mind. The magnitude and distance ranges of the chosen records were defined to be in line with the hazard disaggregation of period ranges utilized for the case-study buildings. During the analysis, the two components of the ground motion were applied to the building and the geometric mean of principal periods, T^*, was used to identify the intensity measure, $Sa(T^*)$. The hazard curves obtained via PSHA were used within the IPBSD framework and, once the acceptable period range was obtained, $\lambda_{c,target}$ was verified by integrating the collapse fragility with the seismic hazard based on an IM of $Sa(T_1)$ for a range of T_1 values, as per Equation (1). The seismic hazard curve corresponding to both sites and a period of $T_1 = 1.0$s is displayed in Figure 7.

3.3 | Eurocode 8

The buildings were designed following the EC8 provisions. For consistency, $Sa(T_1)$ of the elastic design spectrum of EC8 was scaled to match the one obtained from PSHA at the no-collapse return period of 475 years. EC8 does not directly consider performance metrics, such as MAFC and EAL, therefore the values provided in Table 1 were not considered for the case-study applications. As such, only the cases varying in number of storeys and hazard were considered. The equivalent lateral force (ELF) method along with gravity loads was used to estimate the demands on structural elements. Structural element dimensions and reinforcement content was selected to satisfy lateral drift limitation and P-Delta effects. Local ductility limits imposed by EC8 for ductility class medium (DCM) elements were considered. For most elements, minimum local ductility requirements were governing. Cracked cross-section properties (i.e., 50% of gross) were utilised to estimate the demands via the elastic numerical model and design the structural elements. The final design values are listed in Table 2. Additionally, buildings were designed as corresponding to importance classes II and III (i.e., scaling of design spectrum by 1.0 and 1.2, respectively) to distinguish between different levels of safety that are anticipated in the IPBSD designs via the MAFC. Independent of the importance class, the periods associated with both directions are the same, which is due to the same cross-section dimensions. The design code does not directly enforce modification of cross-section dimensions to avoid having the minimum local ductility conditions govern the detailing, therefore a decision was made not to modify the designs.

3.4 | IPBSD formulation

Similar to the case of the EC8 designs, each case study was also designed following the IPBSD framework to meet the stated performance objectives in terms of target MAFC and EAL limit. To better visualize the framework, a single

TABLE 2 Summary of design solutions obtained using EC8

EC8 Case	IPBSD correspondence	Importance class	N_{st}	Seismicity	T_x (s)	T_y (s)	Sa_d (g)
1-EC8	1-IPBSD	II	2	High	0.35	0.35	0.31
2-EC8	4-IPBSD	II	4	High	0.69	0.68	0.13
3-EC8	7-IPBSD	II	6	High	1.11	1.09	0.07
4-EC8	10-IPBSD	II	2	Medium	0.44	0.44	0.11
5-EC8	11-IPBSD	II	4	Medium	0.89	0.88	0.05
6-EC8	12-IPBSD	II	6	Medium	1.42	1.39	0.03
7-EC8	1-IPBSD	III	2	High	0.35	0.35	0.28
8-EC8	4-IPBSD	III	4	High	0.69	0.68	0.15
9-EC8	7-IPBSD	III	6	High	1.11	1.09	0.10
10-EC8	10-IPBSD	III	2	Medium	0.44	0.44	0.13
11-EC8	11-IPBSD	III	4	Medium	0.89	0.88	0.06
12-EC8	12-IPBSD	III	6	Medium	1.42	1.39	0.04

TABLE 3 Performance group contributions to y_{SLS} in % and associated EDPs

Direction	Storey level	θ_S (%)	θ_{NS} (%)	a_{NS} (g)	$y_{S,PSD}$ (%)	$y_{NS,PSD}$ (%)	$y_{NS,PFA}$ (%)
		Initial					
-	Ground floor	–	–	0.44	–	–	0.98
Dir X	1st storey	1.54	0.23	0.51	0.83	1.57	1.32
Dir X	2nd storey	1.54	0.25	0.51	0.82	1.45	0.99
Dir Y	1st storey	1.56	0.20	–	1.44	1.65	–
Dir Y	2nd storey	1.58	0.22	–	1.45	1.51	–
		After the single-step refinement					
-	Ground floor	–	–	0.44	–	–	1.00
Dir X	1st storey	0.23	0.23	0.51	0.00	1.63	0.82
Dir X	2nd storey	0.25	0.25	0.51	0.00	1.38	0.68
Dir Y	1st storey	0.20	0.20	–	0.00	1.72	–
Dir Y	2nd storey	0.22	0.22	–	0.00	1.43	–

case-study application (Case 1-IPBSD) is followed step-by-step herein. It is recalled that $\lambda_{c,target}$ and $\lambda_{y,limit}$ are 2×10^{-4} and 0.60%, respectively, and the location is of high seismicity (L'Aquila).

Initially, performance objectives were defined; the y values of OLS and CLS were fixed to 1% and 100%, respectively, and λ_{OLS} was set to correspond to a limit state return period of 10 years and $\lambda_{CLS} = \lambda_{c,target}$, as illustrated in Figure 2, meaning that only the SLS parameters needed to be defined to respect the limiting EAL. The choice of SLS parameters was analyzed through sensitivity studies in Shahnazaryan et al.[35] and was defined initially as $y_{SLS} = 14\%$ and $\lambda_{SLS} = 1.67 \times 10^{-2}$, which correspond to a loss curve leading to an EAL meeting the EAL limit (i.e., the y_{SLS} was fixed as 14% and λ_{SLS} was iterated until the $\lambda_{y,limit}$ was met). Given these values, the resulting loss curve was identified and λ_y was calculated as the area under the design loss curve as 0.96%, which is exceeding the desired $\lambda_{y,limit}$. However, this slight overestimation was not deemed to be an issue since, as discussed in Section 2.2, a single-step refinement should be made with regard to the actual contributions of different performance groups to y_{SLS}. Note that the SLFs were normalised using a replacement cost of €589,712.40 corresponding to a two-storey building and the relative contributions of different performance groups are given in Table 3, which, when summed, give $y_{SLS} = 14\%$. Costs were computed based on the SLFs corresponding to the critical (lowest) EDP. Subsequent design limits for X and Y directions were obtained as: θ_S of 1.54% and 1.56%; θ_{NS} of 0.23% and 0.20% and a_{NS} of 0.44 g and 0.51 g, respectively.

However, since the design will be based on 0.23% and 0.20% in each direction, as it is the critical PSD value between structural and non-structural groups, the values of 1.54% and 1.56% PSD for structural components will not be exceeded at SLS. Similarly, the design for PFA-sensitive components will be based on 0.44 g in direction X and 0.51 g in direction Y.

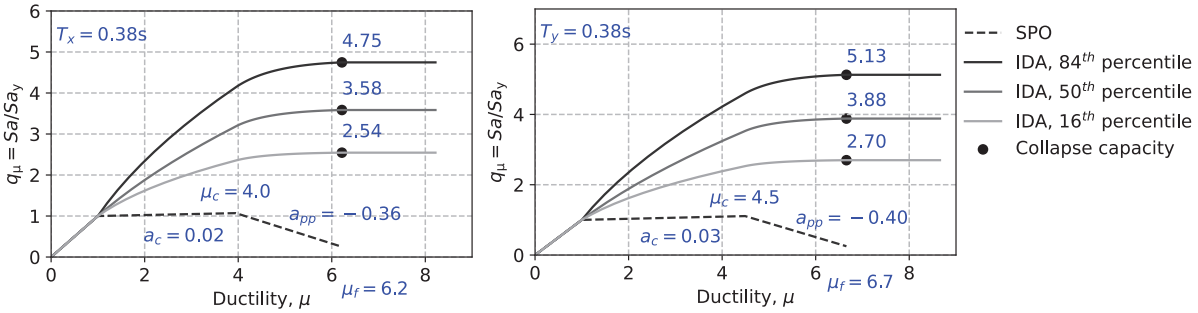

FIGURE 8 SPO and IDA curves obtained via the SPO2IDA tool in (left) X direction, (right) Y direction

Therefore, the single-step refinement discussed in Section 2.2 was made by using 0.23% as the critical PSD for structural component groups as well. To do so, the contributions to costs were recalculated after the refinements based on the EDP value of each level (Table 3), which then summed up to $y_{SLS} = 8.66\%$. This value was used as the new y_{SLS}, and the loss curve was updated effectively resulting in an EAL of 0.60%, thus equal to $\lambda_{y,limit}$. It is interesting to note that the contribution coming from structural components at SLS was effectively zero, which was largely due to the structural members being well-designed and detailed and the SLS loss stemming almost entirely from the non-structural elements.

The feasible period range was identified as between 0.20 s and 0.42 s for the X direction, and 0.20 s and 0.37 s for the Y direction. Following the procedure outlined in Section 2.2, a final design solution with secant to yield periods of 0.38 s in both directions was identified, which is slightly over but within a tolerable difference compared to the upper period limit of 0.37 s for the Y direction. By ensuring the structure has an initial period within a tolerable range with respect to the period range identified, the EAL is expected to be lower than the predefined EAL limit, as it does not reach the period limits, at which excessive losses of drift- or acceleration-sensitive non-structural elements would start to become problematic to the performance objectives (Figure 4C).

Next, collapse safety was controlled via a targeted MAFC. Several assumptions were needed before using the SPO2IDA tool[16] regarding the structural system's expected SPO behaviour, as illustrated in Figure 5(left). However, given the iterative process, all assumptions regarding its shape and secant-to-yield period were established, and the resulting output of SPO2IDA is given in Figure 8, where on the vertical axis q_μ represents the normalization of spectral acceleration, Sa, concerning Sa_y. Only β_{RTR} was considered for what concerns uncertainty. In Figure 8, the SPO2IDA parameters are defined as follows: T_x and T_y are the secant to yield periods in both principal directions of the building; μ_c and μ_f are the hardening and fracturing ductilities; a_c and a_{pp} are the hardening ratio to peak and post-peak softening ratio. The collapse fragility was calculated based on the 50th percentile as the median and the β_{RTR} based on the percentile values shown. The Sa_y was optimised to 0.44 g for both X and Y directions, respectively, meaning that λ_c equated $\lambda_{c,target}$.

With the identified Sa_y, assuming an initial q_s of 1.0, the design base shear was calculated. In each direction separately, design lateral forces were obtained using the ELF method together with gravity loads to perform static analysis and compute element design forces. Strength hierarchy, local ductility requirements and P-Delta effects were all accounted for following the EC8[9] recommendations and structural elements were verified via their moment-curvature relationships using Response-2000[20] and EC2[19] material properties. If any of the sections required cross-section dimension modifications, or the secant-to-yield periods were not within the identified period ranges, or the actual SPO shape varied from the assumed shape initially, the process was repeated. In general, it took from two to five iterations to complete one design. To aid the designer with the workload required for iterations, object-oriented Python-based software[18] has been created, as mentioned in Section 2.3. The final design solutions in terms of T_x, T_y, q_{sx}, q_{sy}, and Sa_d for all case-study buildings considered are shown in Table 4.

For some of the case-study buildings, high values of q_s were observed in both directions. This is predominant for the medium seismicity region, as well as for the cases where local ductility requirements of EC8 governed in terms of minimum reinforcement amount. Thus, independent of Sa_d, the elements had the same moment capacity. In other words, if Sa_d reduced, the q_s subsequently increased. This in turn is a result of having very stiff sections, which could be governed by the period range condition of IPBSD. However, in cases where the period range condition was not too strict, one possible way of avoiding the issue is by decreasing the cross-section dimensions. It is noted that for solutions with high stiffness, masonry infill or RC wall systems could be more optimal to act against seismic loads, the absence of which for moment-resisting RC frames required larger cross-sections for columns and beams, therefore triggering the local ductility and minimum

TABLE 4 Summary of design solutions from the IPBSD

Case	$\lambda_{c,target}$	$\lambda_{y,limit}$ (%)	Seismicity	T_x (s)	T_y (s)	q_{sx}	q_{sy}	Sa_d (g)
1-IPBSD	2.0×10^{-4}	0.60	High	0.38	0.38	1.22	1.17	0.54
2-IPBSD	2.0×10^{-4}	0.80	High	0.52	0.49	5.25	5.64	0.12
3-IPBSD	1.0×10^{-4}	0.60	High	0.37	0.36	7.96	8.22	0.13
4-IPBSD	2.0×10^{-4}	0.60	High	0.66	0.61	1.00	1.00	0.38
5-IPBSD	2.0×10^{-4}	0.80	High	0.95	0.92	1.55	2.16	0.14
6-IPBSD	1.0×10^{-4}	0.60	High	0.71	0.64	1.30	1.70	0.32
7-IPBSD	2.0×10^{-4}	0.60	High	1.25	1.06	2.86	3.80	0.08
8-IPBSD	2.0×10^{-4}	0.80	High	1.36	1.35	1.00	1.00	0.23
9-IPBSD	1.0×10^{-4}	0.60	High	1.20	1.15	1.00	1.00	0.39
10-IPBSD	2.0×10^{-4}	0.60	Medium	0.56	0.60	1.00	1.00	0.22
11-IPBSD	2.0×10^{-4}	0.60	Medium	1.16	1.20	1.00	1.00	0.10
12-IPBSD	2.0×10^{-4}	0.60	Medium	1.41	1.38	1.00	1.00	0.10

reinforcement requirements of EC8 because of relatively low demands. Ideally, the framework allows practitioners to have solutions of different variations and configurations, thus it is not limited to a unique solution or structural typology. Consideration of other structural typologies is not within the scope of this article and will require further research and application.

More conclusions may be drawn from the results displayed in Table 4. Looking at a lower value $\lambda_{c,target}$ of Case 3-IPBSD compared to Case 1-IPBSD, Sa_d is expected to be lower for the latter case but is seen to be notably higher. This could be attributed to the variation of ductilities as well as q_s. In other words, ductilities and q_s in both directions are higher for Case 3-IPBSD, thus the target MAFC may be met with lower Sa_d. So, while the two performance objectives are verified within two parts of the IPBSD framework, there is still an indirect relationship between the two. This relationship is more apparent when the period range is more stringent. It is a combination of $\lambda_{c,target}$, $\lambda_{y,limit}$, seismic hazard as well as initial secant-to-yield period (controlled by the stiffness of the structure), and the backbone shape that results in an efficient loss-driven risk-targeted design. To test this statement, Case 3-IPBSD was forced to have structural systems in each direction with a T_x and T_y of 0.65 s and 0.61 s, respectively. As a result, the new Sa_d was identified as 0.33 g as a direct impact of seismic hazard and period. While this is only slightly higher than Sa_d of Case 1-IPBSD, one should not forget about the SPO shape, which is characterised by a certain ductility value as well. Essentially, choices before and during the IPBSD framework will dictate how the building design solution will shape up, simultaneously without hindering the ability of the IPBSD framework to provide solutions meeting the desired performance objectives.

4 | STOREY LOSS FUNCTIONS

As mentioned previously, in order to implement the IPBSD framework, SLFs need to be provided. The SLF toolbox proposed by Shahnazaryan et al.[15] was utilised to generate SLFs for residential occupancy of the entire building. To estimate the replacement cost of the case-study buildings, a mean unit cost of €1213.40 related to RC buildings in L'Aquila was adopted from Di Ludovico et al.[36] Components sensitive to only two engineering demand parameters (EDPs), PSD and PFA, were considered within the component inventory of the case-study buildings. Components of the same sensitivity in one direction of seismic action, same EDP sensitivity and located within the same storey level were grouped into the same performance group, while non-directional components were grouped into a different performance group following the same reasoning. Cost distributions for the structural and non-structural components, quantities as well as fragility function sources are summarised in Tables 5–7. The component inventory was built based on design drawings following an idealized building layout (Figure 6) that was adopted as case-study for the purposes of implementation and validation of the IPBSD framework. The tables provide information on the type of component, the demand parameter to which they are sensitive, the units and quantities for each type of component. Components for which a second number between parenthesis is missing are sensitive to the seismic action of both directions. For a detailed component inventory, readers are referred to the additional sample files available on GitHub.[18]

TABLE 5 Mean quantities for the damageable PSD-sensitive structural components in the X (Y) direction

Component	Fragility function source	Consequence function source	Unit	Quantities per storey	
				Ground	Typical
External columns	FEMA P58-3[37]	Cardone[38]	each	4	4
Internal columns	FEMA P58-3[37]	Cardone[38]	each	4(10)	4(10)
Central columns	FEMA P58-3[37]	Cardone[38]	each	10	10

TABLE 6 Mean quantities for the damageable PSD-sensitive non-structural components in the X (Y) direction

Component	Fragility function source	Consequence function source	Unit	Quantities per storey	
				Ground	Typical
Exterior masonry infill	Cardone & Perrone[39]		m^2	84 (168)	72 (144)
Internal masonry partitions	Cardone & Perrone[39]		m^2	67.8 (59.8)	32.3 (24.2)
Internal masonry infill partitions	Sassun et al.[40]		m^2	138.5 (80.4)	118.7 (68.9)
Non-monolithic precast concrete stair assembly	FEMA P58-3[37]		each	1	1
Doors	Correlated to the collapse of internal masonry partitions	Market research	each	6(6)	6 (6)
Windows			each	2(13)	2 (13)
Chairs			each	18	18
Oven with cooker			each	2	2
Fridge			each	2	2
Washing machine			each	2	2

The selection of representative fragility and consequence functions is a complex issue and could be a cause of inaccuracy when conducting loss assessment. However, it is not within the scope of this study to provide reference component inventory and loss assessment results, but rather demonstrate the capabilities of the IPBSD framework given the input arguments in terms of SLFs. Existing fragility and consequence functions[38–40] were adopted for structural and non-structural components in RC structures. The costs associated with structural components are associated with existing structures, whereas the repair actions are assumed to be the same for newly designed structures and the fragility functions must accommodate for ductile beam-column subassemblies. Fragility and consequence functions of PFA-sensitive components, as well as of stairs, were adopted from FEMA P58.[37] In addition, consequence functions of components from FEMA P58 use a conversion of 0.79 based on the work by Silva et al.,[41] which are further multiplied by 0.83 to reflect the conversion of USD to EUR as of January 2021.

For some non-structural components, specific fragility and consequence functions were not available thus some assumptions were made using engineering judgement. For example, PSD-sensitive components with missing fragility information were correlated to the fragility functions assumed for partition walls. Similarly, PFA-sensitive components with missing fragility information were correlated to the fragility functions of piping systems. The logic behind the correlations lies within the assumption that damaged or collapsed partition walls will inadvertently damage the windows or doors located within the walls, while the leakage of piping systems would result in damage to electronics or furniture, as discussed in De Risi et al.,[42] for example. The costs associated with those components were adapted from typical values of available market prices in Italy.

Figure 9 illustrates sample SLFs for the 2nd level of the case-study building's plan layout. Losses of NS components start rising at low values of PSD, which may be attributed to the low capacities of interior and exterior infills. In contrast, structural components' costs start accumulating once a certain threshold of PSD is reached, which is a direct result of the high capacities of well-designed ductile beam-column sub-assemblies. For what concerns the Y of different performance groups utilized in Equation (4), as an example, the Y values for a two-storey building were: 12% and 21% for PSD-sensitive

TABLE 7 Mean quantities for the damageable PFA-sensitive non-structural components

Component	Fragility function source	Consequence function source	Unit	Quantities per floor		
				Ground	Typical	Roof
Fancoil	FEMA P58-3[37]	FEMA P58-3[37]	each	0	8	8
Ceiling system			m^2	0	274.5	288.0
Lighting			each	0	19	19
Piping – water distribution			250 m	0	0.605	0.605
Piping – heating distribution			250 m	0	0.638	0.638
Sanitary waste piping			250 m	0	0.605	0.605
Bookshelves	Correlated to the collapse of piping distribution systems	Market research	each	0	6	6
Wardrobes			each	0	8	8
Sofas			each	0	4	4
Tables			each	0	8	8
Shelves			each	0	11	11
Beds			each	0	6	6
Kitchen equipment			each	0	2	2
Computers			each	8	8	0
TV			each	4	4	0
Fire sprinkler water piping	FEMA P58-3[37]	FEMA P58-3[37]	250 m	0	0.5184	0.5184
Fire sprinkler drop			each	0	12	12
Distribution panel			each	1	1	0
Hydraulic elevator			each	1	0	0
Battery rack			each	1	0	0
Battery charger			each	1	0	0
Distribution panel for the elevator			each	1	0	0

structural components in directions 1 and 2, respectively, 22% for PSD-sensitive non-structural components in both directions, and 23% for PFA-sensitive non-structural components.

5 | STRUCTURAL PERFORMANCE AND LOSS ASSESSMENT RESULTS

In order to thoroughly investigate and validate the designs described previously, each case-study building was modelled as described in Section 3.1 and IDA was performed to characterise the structural behaviour up to lateral collapse using the ground motions described in Section 3.2. Based on the IDA outputs, the SLF-based loss assessment was carried out, using the approach proposed by Ramirez and Miranda.[43] The economic loss conditioned on the ground motion intensity was computed as the summation of the following losses: building collapse; repair costs associated with damageable components of the building; and losses because of demolition of the building due to excessive residual drifts. For the case-study applications, the probability of demolition of a building as a function of residual peak storey drift was assumed to be log-normally distributed with a median of 0.015 and a logarithmic standard deviation of 0.3.[43] Even though low residual drifts are expected, in line with common practice, these were included in the assessment, confirming the expected low contribution of demolition to direct losses in newly designed buildings, following the IPBSD framework. The λ_y was computed by integrating the vulnerability curve, expressed in terms of expected direct economic loss as a function of $Sa(T^*)$, with the site hazard curve at a corresponding geometric mean of principal periods, T^* (Equation (2)). Using these extensive analysis outputs, the actual λ_c and λ_y values were compared to $\lambda_{c,target}$ and $\lambda_{y,limit}$, respectively, to assess each method in delivering sufficiently safe and uniform risk design solutions. The λ_c and λ_y values were computed using the hazard described in Section 3.2 and are presented in Table 8 and illustrated in Figure 10.

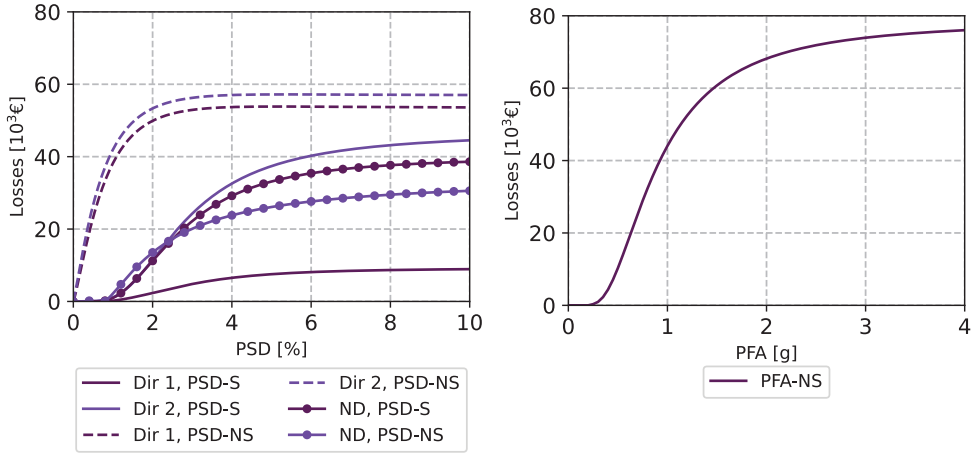

FIGURE 9 SLFs for the case-study building's (left) 2nd storey level for PSD-sensitive elements and (right) 2nd floor for the PFA-sensitive elements

TABLE 8 Summary of actual λ_c and λ_y for each case-study building and design approach considered

IPBSD Cases	λ_c	λ_y (%)	EC8 cases	λ_c	λ_y (%)
1-IPBSD	1.1×10^{-4}	0.56	1-EC8	1.5×10^{-4}	1.14
2-IPBSD	1.8×10^{-4}	0.69	2-EC8	2.3×10^{-4}	0.88
3-IPBSD	1.0×10^{-4}	0.66	3-EC8	2.8×10^{-4}	1.01
4-IPBSD	0.6×10^{-4}	0.50	4-EC8	0.5×10^{-4}	0.58
5-IPBSD	2.2×10^{-4}	0.72	5-EC8	0.5×10^{-4}	0.49
6-IPBSD	0.6×10^{-4}	0.51	6-EC8	0.4×10^{-4}	0.44
7-IPBSD	1.4×10^{-4}	0.52	7-EC8	1.4×10^{-4}	0.96
8-IPBSD	1.3×10^{-4}	0.58	8-EC8	2.3×10^{-4}	0.87
9-IPBSD	0.9×10^{-4}	0.58	9-EC8	2.9×10^{-4}	1.02
10-IPBSD	0.4×10^{-4}	0.31	10-EC8	0.5×10^{-4}	0.58
11-IPBSD	0.3×10^{-4}	0.32	11-EC8	0.7×10^{-4}	0.49
12-IPBSD	0.2×10^{-4}	0.27	12-EC8	0.4×10^{-4}	0.44

It could be argued from Figure 10 that, in terms of MAFC, the EC8-designed buildings demonstrate good results when compared to the IPBSD cases. While true, this stems from the fact that most of the EC8 cases, independent of importance class, have been overdesigned due to governing local ductility requirements regarding minimum required reinforcement. Consequently, a similar backbone behaviour has been observed for most of the EC8-designed cases. Additionally, the EC8-designed cases were anticipated to have MAFC and EAL not far off the target and limit values set for the IPBSD cases, since these were set based on the actual attained values from the literature, as described in Section 3.1.

5.1 | Buildings designed according to EC8

Performance metrics obtained for the case-study buildings designed following EC8 recommendations were at a similar level. MAFC values ranged from 1.5 to 3.0×10^{-4} and 0.4 to 0.7×10^{-4} for cases located in high and medium seismicity regions, respectively. Similarly, values of EAL ranged from 0.88 to 1.15% and 0.44 to 0.58% for high and medium seismicity regions, respectively. Very minor variations were observed in terms of the selected importance class. Hence, there is no indication of improved performance with increased importance class as per EC8. This could be attributed to buildings of the same configurations sharing the same periods as well as having minimum local ductility requirements governing the design. In other words, for the medium seismicity region, the buildings had lower overstrength compared to the high seismicity region, while the dimensions and reinforcement content of sections remained intact. Similarly, no significant

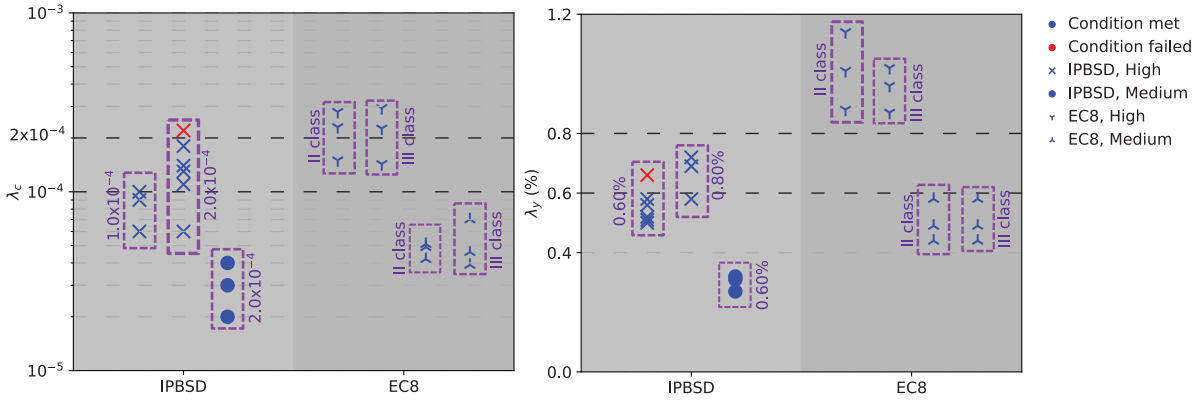

FIGURE 10 Illustration of λ_c and λ_y values for each case-study building and design approach considered

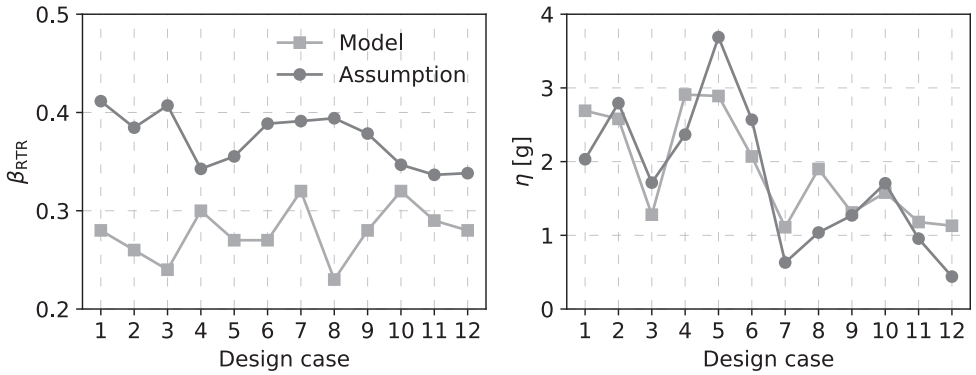

FIGURE 11 Comparison of computed and assumed values of (left) β_{RTR} and (right) η at CLS

variation of EAL values was observed for the buildings located in the medium seismicity region as the variations of Sa_d given in Table 2 were not significant enough. While it is possible to achieve variations of design within the limits allowed by EC8 through the modification of reinforcement content and cross-section dimensions, it is important to note that, due to the absence of direct consideration of MAFC and EAL objectives during design, a practitioner is not forced to modify the design solution. Therefore, the solutions obtained here are some of the possible outcomes following the EC8 recommendations, which highlights the need for the development of risk-targeted procedures.

5.2 | Buildings designed using IPBSD

5.2.1 | Collapse safety assessment

Regarding the IPBSD framework, consistent results were obtained in terms of satisfying both performance objectives (i.e., EAL limit and MAFC target) for each case-study building as shown in Figure 10, whereby both primary performance objectives were met. However, it is important to note that performance objectives were not always close to those identified before the design. While demonstrating the efficiency of the IPBSD framework, minor adjustments could be made to narrow the gap between the actual and target or limit values of performance objectives. One of the possible reasons for the variation could be attributed to the use of SPO2IDA, which was not developed accounting for bidirectional effects, but rather a one-dimensional response. The values of λ_c were computed using the seismic hazard at the geometric mean of the periods from two principal modes (X and Y directions) of the building. Figure 11 provides the medians, η, and β_{RTR} of the collapse capacities of the design cases. A high variation of β_{RTR} is observed, while the values of η were within tolerable proximity of each other. It is interesting to note that even for the cases where η was lower than the assumption, due to the corresponding value of β_{RTR} being lower, the MAFC condition was still met.

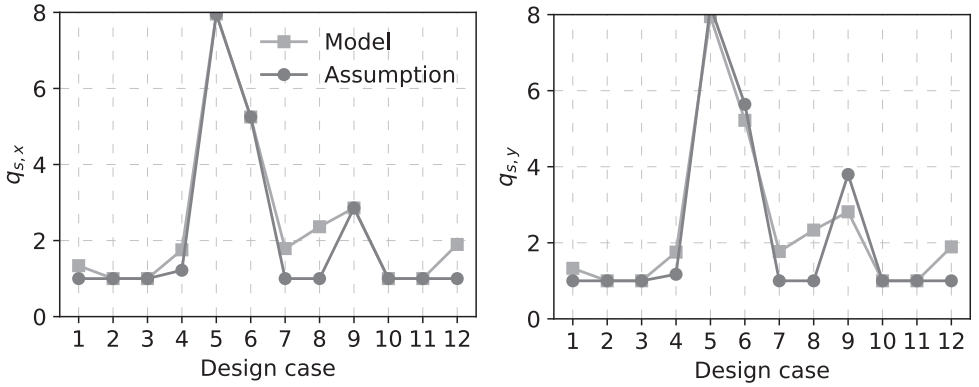

FIGURE 12 Comparison of computed and design values of q_s

TABLE 9 Summary of revised (R) case-study buildings located in medium seismicity region

Case	T_x (s)	T_y (s)	q_{sx}	q_{sy}	Sa_d (g)	η (g)	β_{RTR}	λ_c	λ_y (%)
10-IPBSD-R	0.42	0.43	1.14	1.00	0.51	2.44	0.25	0.2×10^{-4}	0.30
11-IPBSD-R	0.77	0.72	1.00	1.00	0.35	1.96	0.32	0.2×10^{-4}	0.31
12-IPBSD-R	1.31	1.20	1.00	1.00	0.18	1.31	0.29	0.2×10^{-4}	0.27

Similarly, Figure 12 demonstrates the values of q_s (for both directions, q_{sx} and q_{sy}) during design and the actual values obtained from the non-linear model. Several of the cases where actual q_s was higher than 1, while the assumption was equal to 1. Essentially, minimum local ductility requirements were governing, meaning that the sections were larger than necessary, and the demands were subsequently low. However, there is a necessity to keep those cross-sections to satisfy the period condition. In that case, if the assumed overstrength is increased the yield strength will reduce, meaning that in the next iteration, q_s will be even larger, since the minimum ductility condition will be even more relevant with newly reduced demands. Accordingly, this is a cycle, where no convergence could be achieved therefore it was forced to have $q_s = 1$, which is why for many of those cases the MAFC condition is met with a larger than the anticipated gap. In addition, larger variations of λ_c compared to $\lambda_{c,target}$ was observed due to the building failing in either of the directions depending on the ground motion record pair.

5.2.2 | Loss assessment

One of the critical aspects to examine in this work was the IPBSD's ability to actually limit the EAL. So far, only conceptual considerations have been made in the literature without detailed verifications, which are presented in this section.

For most of the cases, λ_y were below $\lambda_{y,limit}$ and only for a single case the limit was exceeded and the performance objective was not met. Furthermore, case-study buildings of a medium seismicity region demonstrated consistently very low values of λ_y regardless of the $\lambda_{y,limit}$. This is primarily due to the lower hazard, which is not likely to cause high losses despite the well-designed and risk-targeted design solutions. At the same time, this is an indication of possible directions to optimise the designs, if a λ_y closer to the limit is desired. For example, the medium seismicity buildings may be revised to have stiffer structural systems or different structural typologies may be sought (e.g., with masonry infills or RC walls as the main lateral load resisting system). To test such a hypothesis, the cases associated with medium seismicity were redesigned and reassessed with stricter performance objectives, that is, 0.5×10^{-4} and 0.40% for target MAFC and EAL limits, respectively. The results for these new case-study buildings are given in Table 9, where it can be seen how the computed λ_y and λ_c are closer to the new performance objectives. As mentioned, this was a direct impact of lower seismic hazard and modern design code provisions, as higher values of performance objectives were not likely to be attained with the current structural typology in hand. However, it is important to note that IPBSD was able to ensure that the performance objectives set by the practitioner were met for both scenarios. As expected, stricter performance objectives resulted in higher requirements in terms of collapse capacity. However, the period limits and therefore periods associated with both directions, T_x and T_y, were largely unaffected, which is again attributed to lower seismic hazard, for which

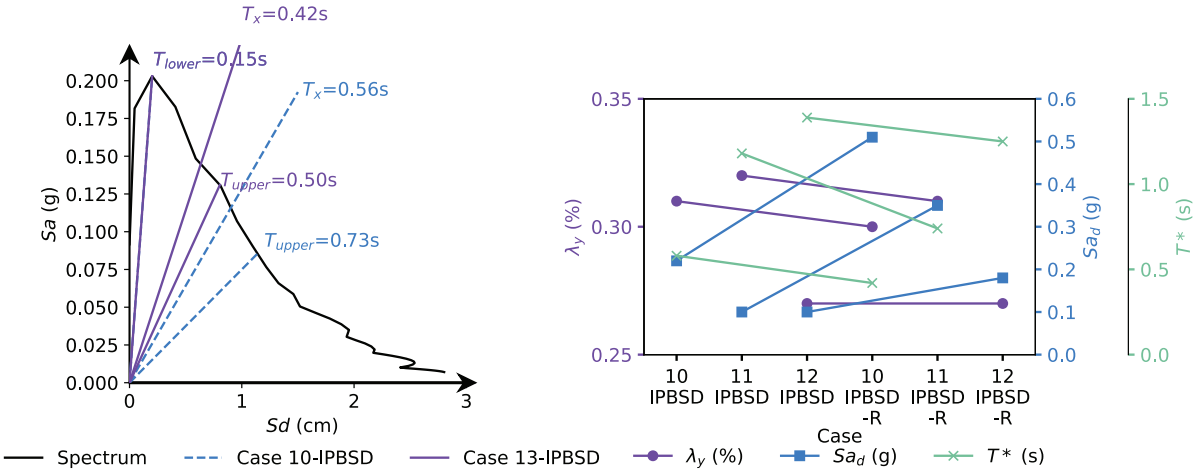

FIGURE 13 (left) Period limits in X direction and (right) Variation of design solutions through the modification of performance objectives, where three distinct lines corresponding to three separate axes are superposed for graphical correspondence

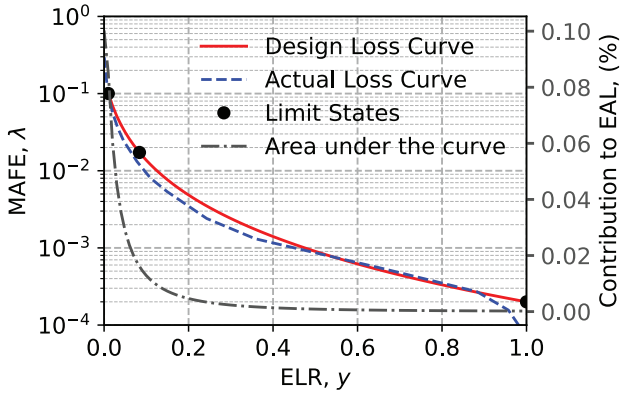

FIGURE 14 Loss curves for case 1-IPBSD

the periods are still within the limits. Further restriction of $\lambda_{y,limit}$ to lower values will likely result in a direct impact for significant variations in periods.

Figure 13(left) demonstrates the variations of period limits in X direction for case 10-IPBSD, and through the subsequent modification of $\lambda_{y,limit}$ for case 10-IPBSD-R. While T_{lower} was unaffected due to no further constraint towards acceleration sensitive components, T_{upper} has decreased from 0.73 s to 0.50 s, meaning that a target period of 0.56 s is no longer satisfactory. The new building has a period of 0.42 s in X direction, as listed in Table 9. To further visualise the impact of stricter performance objectives, Figure 13(right) plots the change in λ_y, Sa_d and the geometric mean of principal periods, T^*, for the paired cases. As expected, Sa_d is larger for cases with stricter performance objectives, while, for the contrary conditions, T^* is reducing. However, while true for cases 10-IPBSD and 11-IPBSD, λ_y did not decrease for 10-IPBSD-R. The slight reduction of λ_y for two of the cases indicate the improvement of building performance through stricter performance objectives, however, as discussed earlier, the goal was not to improve performance but rather have λ_y closer to $\lambda_{y,limit}$ for the medium seismicity region.

The design loss curve was then compared to the actual loss curve for case 1-IPBSD in Figure 14, denoting quite a good match. For comparative purposes, the actual loss curve was computed without considering demolition and collapse loss contributions. As anticipated, when plotting the area under the actual loss curve with respect to ELR, the bulk of the contribution to EAL comes at lower ELR values, where the corresponding MAFE is significantly larger. In addition, while easily disregarded, the selection of the OLS point, that is, its return period, is important, as the contribution of high-frequency seismic events could have a significant contribution to the EAL of the building. Therefore, the return period at the OLS may be further reduced to have a better representation of the actual loss curve during the design stage. In contrast,

TABLE 10 Summary of IPBSD results for a single seismic frame

Solution ID	T_1 (s)	Sa_{SLS} (g)	λ_y (%)
1-IPBSD-2D	0.74	0.143	0.79
2-IPBSD-2D	0.69	0.143	0.68
3-IPBSD-2D	0.64	0.169	0.68
4-IPBSD-2D	0.60	0.169	0.60
5-IPBSD-2D	0.54	0.207	0.65
6-IPBSD-2D	0.52	0.207	0.62
7-IPBSD-2D	0.46	0.207	0.49
8-IPBSD-2D	0.42	0.254	0.55
9-IPBSD-2D	0.39	0.254	0.50
10-IPBSD-2D	0.29	0.304	0.41
11-IPBSD-2D	0.35	0.254	0.39
12-IPBSD-2D	0.23	0.356	0.34
13-IPBSD-2D	0.20	0.356	0.32

the contribution to EAL at large ELRs is negligible, even if the loss curve mismatch further highlights the importance of high frequency events for computation of losses.

6 | DETAILED ANALYSIS OF LOSS ESTIMATES

6.1 | Secant-to-yield (T_1) period range considerations

To better understand how the assumptions involved within the IPBSD framework affected the actual loss computations and their accuracy, the results were scrutinised to understand the loss contributions of different performance groups at the SLS. Moreover, the variation of EAL was explored by modifying the initial secant-to-yield period, T_1. Since this method's inception in O'Reilly and Calvi,[8] the effect of T_1 has not yet been thoroughly examined via actual analysis data but rather conceptual considerations and logic. Therefore, the results included in this section provide such evidence. For the analysis, performance objectives were set to 1.0×10^{-4} and 0.8%, for λ_c and λ_y, respectively, however only λ_y will be focused on herein. As mentioned in Section 5.2.2, the return period at OLS is a non-trivial point and was reduced to 5 years to better capture the actual loss curve at the design stage, while the return period at SLS was assumed to be 60 years. SLFs were generated for a three-storey residential RC building with two seismic frames similar to the layout presented in Figure 6 but assuming a *perimeter* seismic resisting system which is more suitable for two-dimensional analysis given the symmetry of the layout. Therefore, only one direction was analysed for simplicity to directly visualise the contributions to loss. IPBSD was applied as originally foreseen to identify the initial secant-to-yield period range within 0.24 s and 0.53 s, corresponding to a PFA of 0.43 g and PSD of 0.22%, respectively. Loss contribution ratios amounted to 0.57 and 0.43 for non-structural PSD-sensitive and PFA-sensitive components, respectively. The ratio for structural components was significantly lower (i.e., <0.01). Also, a decision not to meet the period range condition was made to analyse its impact on loss variations when not met. IDA and loss assessment was performed for each solution as conduced in previous sections. Table 10 provides the EAL values for each considered T_1. As observed, the EAL limit was met for all solutions. Additionally, EAL tends to decrease with decreasing T_1 (Figure 15), indicating that the more flexible structures tend to accumulate more losses, which is a reflection of SLF contributions outlined in Section 3.4. In contrast, if the acceleration-sensitive components were more to increase in value (with no change in fragility), the decrease in EAL will be less apparent, as the loss contributions of those components would be higher in comparison with displacement-sensitive components.

At Sa_{SLS} values for each solution provided in Table 10, loss contributions were evaluated to see how the assumptions faired. As expected, demolition and collapse loss contributions proved to be negligible at SLS design intensity, which relates to direct economic loss only and not to other factors, such as downtime and indirect losses. Therefore, they were not considered, and the remaining performance group losses were normalised by the total costs (Figure 15 and Table 11). At lower periods, the significant contribution to total losses comes from PFA-sensitive components, while, with increasing

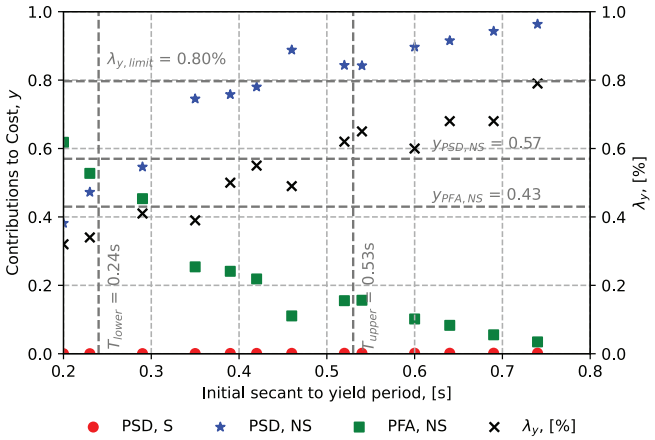

FIGURE 15 Loss contributions of different performance groups to the total repair cost at SLS

TABLE 11 Loss contributions and T_1 of different performance groups to the total repair cost at SLS

Solution ID	T_1 (s)	PSD, S (%)	PSD, NS (%)	PFA, NS (%)
1-IPBSD-2D	0.74	0.2	96.3	3.5
2-IPBSD-2D	0.69	0.2	94.3	5.5
3-IPBSD-2D	0.64	0.2	91.5	8.3
4-IPBSD-2D	0.60	0.2	89.6	10.2
5-IPBSD-2D	0.54	0.1	84.3	15.6
6-IPBSD-2D	0.52	0.1	84.4	15.5
7-IPBSD-2D	0.46	0.1	88.8	11.1
8-IPBSD-2D	0.42	0.1	78.0	21.9
9-IPBSD-2D	0.39	0.1	75.8	24.1
10-IPBSD-2D	0.29	0.0	54.7	45.3
11-IPBSD-2D	0.35	0.1	74.5	25.4
12-IPBSD-2D	0.23	0.0	47.3	52.7
13-IPBSD-2D	0.20	0.0	38.2	61.8

T_1, the loss contributions associated with PSD-sensitive non-structural (NS) components start increasing. In contrast, the loss contributions from PSD-sensitive structural (S) components were negligible, which confirmed the considerations made in Figure 3. The actual loss contributions did not quite match the assumed ones through the design process, which is primarily due to having the same design EDP along the height of the building, which will be further explored in Section 6.2. As expected, with the increase of the initial secant-to-yield period, the loss contributions from PFA-sensitive components decrease, while the contributions due to PSD-sensitive components increase. It is important to note that the period range is not a direct representation of precise loss contributions. For example, the upper period limit is based on the critical PSD, while the lower period limit is based on the critical PFA. This means that, during design, reasonably high values of 0.57 and 0.43 for PSD- and PFA-sensitive component groups, respectively, will be assumed. However, it is not reasonable to expect high loss contributions from PFA-sensitive components at the upper period limit, whereas the opposite is true at the lower period limit. The compromise between both component groups ensures that the losses will not be exceeded within the period range.

From Figure 15, one may infer that the computed λ_y is expected to be closer to $\lambda_{y,limit}$ at the vicinity of T_{lower}, where the component group contributions are in the vicinity of values obtained during design (i.e., 0.57 and 0.43 for PSD- and PFA-sensitive components, respectively). However, while the contributions in terms of ratios are expected, the actual EAL contribution values in terms of percentage are lower than expected. This is a direct impact of the period where there is always a compromise. That is, the limits are set based on discrete values of PFA and PSD during design, while it is highly unlikely to have critical PSD (associated with T_{upper}) when critical PFA (associated with T_{lower}) was estimated. The goal of

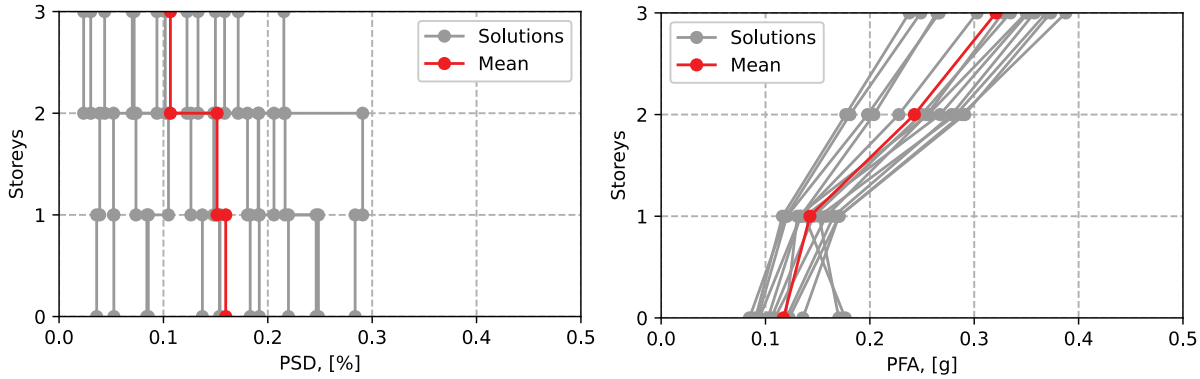

FIGURE 16 PSD and PFA profiles along with the height of the structure at SLS

TABLE 12 Updated EDP profiles and corresponding y values

Floor/Storey	PSD, NS [%]	PFA, NS (g)	$y_{PSD,NS}$ (%)	$y_{PFA,NS}$ (%)
0	–	0.16	–	0.00
1	0.22	0.19	1.81	0.03
2	0.21	0.33	1.46	0.25
3	0.15	0.43	0.99	0.74

the framework is not to optimize for $\lambda_{y,limit}$, but rather ensure that period range is not disrupted, hence, losses associated with component groups of both EDP-sensitivities are not exceeded.

6.2 | Influence of the EDP profiles

To further understand possible improvement paths, the EDP profiles of the solutions were plotted in Figure 16. PSD averages around 0.15% for all solutions at the first two storeys and 0.10% at the third storey level, while the value used in IPBSD was 0.22%. In contrast, the PFA profile varies between 0.1 and 0.4 g, while, during the application of IPBSD, a value of 0.43 g was observed at SLS. A possible improvement for this is the utilisation of reduction factors during design to account for possible variations of EDP values at different storeys. However, empirical equations available in the literature[13] generally assume a reduction of PSDs along the height, while here, as observed, PSDs at the first and second storeys were nearly equal. As such, a decision was made not to implement PSD reduction factors. On the other hand, this may be of more importance for PFA-sensitive components, as there is a notable discrepancy of values along the height of the building. To aid that, recent simplified methodologies based on a modal superposition approach[44,45] may be investigated in the future to estimate floor accelerations more accurately.

Instead of using predefined EDP profiles based on empirical equations available from the literature, the PSD and PFA profiles obtained in Figure 16 were used as benchmarks to scale the design EDPs accordingly. The updated EDPs and corresponding y values at SLS are given in Table 12. The EDP values at each storey or floor level were scaled based on the mean profiles presented in Figure 16 resulting in reduced y values, therefore, the loss curve was subsequently updated and the new EAL limit was set to 0.58%. None of the solutions having a period larger than the upper period limit (Table 10) met the new EAL limit, demonstrating the non-conservative, yet optimized, nature of the modification. The same does not hold for a solution with a period below the lower period bound, which could be attributed to significant reductions of losses associated with PSD-sensitive components, as opposed to an increase in losses associated with PFA-sensitive components.

Finally, the loss curves for all the case-study frames were plotted together with the design loss curve, identified via the IPBSD framework, in Figure 17. As one may note, the larger variations are for high return periods (low MAFE levels). This indicates a possible improvement when fitting the design loss curve at the outset. However, similar to the findings in Section 5.2.2, this option was not adopted, as the variations at high return periods do not significantly affect EAL, which is more sensitive to events associated with low return periods as shown in Figure 14. Furthermore, the loss curve before the

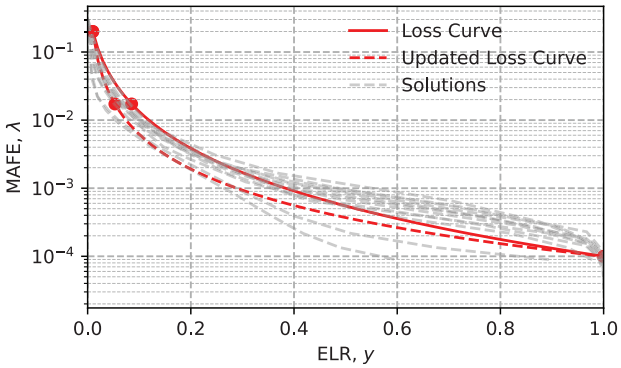

FIGURE 17 Comparison of loss curves for the 2D frames with the initial and updated loss curves

modifications through the reduction factors has an ELR at SLS that is higher than the one of any of the actual loss curves, which is an indication of lower EALs compared to the design or limit.

7 | SUMMARY AND CONCLUSIONS

This article described and validated an integrated performance-based seismic design (IPBSD) framework, based on the fundamental objectives of performance-based earthquake engineering (PBEE), that aims to design buildings by limiting expected monetary losses while targeting acceptable collapse safety. The IPBSD framework was applied to several case-study reinforced concrete (RC) frame buildings, for which the structural elements were designed and numerical models developed to perform non-linear incremental dynamic analysis (IDA). The IDA response of each building was then used to assess the collapse safety and perform loss assessment with the ultimate goal of estimating expected annual loss (EAL) and comparing it with the limit initially set for the IPBSD implementation. Similarly, Eurocode 8 provisions were applied, and an additional set of frames were designed for comparative purposes with respect to the IPBSD framework. The main conclusions of this study are as follows:

- The case-study application of IPBSD to several buildings again showed good results in terms of meeting the MAFC target (Section 5.2.1), which was previously shown,[6] in addition to meeting the EAL limit and matching the design loss curves scrutinised here (Section 5.2.2);
- All of the Eurocode 8-designed case-study buildings demonstrated mean annual frequency of collapse (MAFC) values similar to the ones found in the literature. Buildings of importance class III exhibited improved performance in neither collapse safety nor loss reduction in a significant manner when compared to buildings of importance class II. This is primarily due to the chosen configurations and local ductility requirements in terms of minimum element reinforcement that governed the design. Furthermore, this also denotes the wide variety of possible design solutions via Eurocode 8 provisions, when specific criteria to achieve risk and loss-targeted solutions are not foreseen;
- The comparison of the multiple loss curves with the design loss curve in Section 5.2.2 indicated the need for refining the first limit state point, that is, operational limit state, through the reduction of its return period. This stemmed from larger contributions to EAL at frequent seismic events associated with high return periods and contributions from the structural performance group;
- A simpler refining measure for the establishment of expected loss ratios and EAL using the critical EDP (associated with non-structural or structural component groups) was implemented. Compared to the previous versions of the framework, the refined approach of re-computing the EAL is less conservative and not far from the limit EAL initially set out, which represents a notable improvement;
- The effects of the assumptions on the performance of buildings in terms of limiting economic losses were further assessed. It was shown in Section 6.2 that the assumption of uniform EDP profiles at the design stage is not representative of actual EDP profiles. Consequently, the mean EDP profiles of all buildings were used to generate reduction factors and reapplied at the design stage. The updated loss curve resulted in a reduction of limiting EAL by around 25%. In lieu of generated reduction factors, empirical equations available from the literature may be used to perform the reductions for more optimised and less conservative EAL limit identification;

- The IPBSD framework, applied in a Python-based object-oriented environment, yielded consistent results in terms of meeting the performance objectives of both MAFC and EAL. It was demonstrated through the application of the framework on multiple case-study RC buildings and validated through its bidirectional response and loss assessment. Regardless of the seismic hazard, number of storeys and performance objective levels, the performance of the IPBSD framework was consistently satisfactory;
- Some of the assumptions within the IPBSD framework require further research and parametric studies for more optimised designs that require less computational effort. The anticipated collapse capacity uncertainty, β_{RTR}, proved to be significantly higher than the actual ones obtained through IDA. This is primarily related to its computation being based on three distinct points of the collapse fragility curve during design (in the absence of all points given by a specific tool (e.g., SPO2IDA)) whereas, during the assessment, the whole spectrum of points on the fragility curve is used for a more precise computation.

Overall, the IPBSD framework performs well hence is suitable for the next-generation seismic design approaches meeting the goals of PBEE. The flexibility and simplicity of the framework in achieving risk-consistent and loss-driven designs lie within its ability to combine advantages of various methods available in the literature, with the inclusion of code-based provisions. The parametric investigations described here serve to illustrate the applicability of the method and also the aspects for which there is still room for improvement.

ACKNOWLEDGEMENTS

The work presented in this paper has been developed within the framework of the project "Dipartimenti di Eccellenza", funded by the Italian Ministry of Education, University and Research at IUSS Pavia.

DATA AVAILABILITY STATEMENT

The data that support the findings of this study are openly available in GitHub at https://doi.org/10.5281/zenodo.5035061, Ref. 17

ORCID

Davit Shahnazaryan https://orcid.org/0000-0002-0529-5763
Gerard J. O'Reilly https://orcid.org/0000-0001-5497-030X
Ricardo Monteiro https://orcid.org/0000-0002-2505-2996

REFERENCES

1. SEAOC. *Vision 2000: Performance-based Seismic Engineering of Buildings 1995*.
2. Cornell CA, Krawinkler H. Progress and challenges in seismic performance assessment. *PEER Center News*. 2000;3(2):1-2.
3. Cornell CA, Jalayer F, Hamburger RO, Foutch DA. Management agency steel moment frame guidelines. *J Struct Eng*. 2002;128:526-533.
4. FEMA. seismic performance assessment of buildings – methodology. *Fema P-58-1*. 2012;1(September):278.
5. CNR. Istruzioni per la valutazione affidabilistica della sicurezza sismica di edifici esistenti. *CNR – Commissione Di Studio per La Predisposizione e l'analisi Di Norme Tecniche Relative Alle Costruzioni* 2014.
6. Shahnazaryan D, O'Reilly GJ. Integrating expected loss and collapse risk in performance-based seismic design of structures. *Bull Earthquake Eng*. 2021;19(2):987-1025.
7. Vamvatsikos D, Kazantzi AK, Aschheim MA. Performance-based seismic design: avant-garde and code-compatible approaches. *ASCE-ASME J Risk Uncert Eng Syst A: Civil Eng*. 2016;2(2). https://doi.org/10.1061/AJRUA6.0000853.
8. O'Reilly GJ, Calvi GM. Conceptual seismic design in performance-based earthquake engineering. *Earthquake Eng Struct Dyn*. 2019;48(4):389-411.
9. CEN. *Eurocode 8: Design of Structures for Earthquake Resistance - Part 1: General Rules, Seismic Actions and Rules for Buildings (EN 1998-1:2004)*. Brussels, Belgium: 2004.
10. NZS. *NZS 1170.5 Supp 1:2004 - Structural Design Actions Part 5: Earthquake Actions - New Zealand - Commentary*. Wellington, New Zealand: 2016.
11. ASCE 7–16. *Minimum Design Loads for Buildings and Other Structures*. 2016.
12. Priestley MJN. *Myths and Fallacies in Earthquake Engineering, Revisited*. IUSS Press; 2003.
13. Priestley MJN, Calvi GM, Kowalsky MJ. *Displacement Based Seismic Design of Structures*. IUSS Press; 2007.
14. Sullivan TJ, Calvi GM, Priestley MJN, Kowalsky MJ. The limitations and performances of different displacement based design methods. *J Earthquake Eng*. 2003;7(2014):201-241. August.
15. Shahnazaryan D, O'Reilly GJ, Monteiro R. Story loss functions for seismic design and assessment: development of tools and application. *Earthquake Spectra*. 2021;37:2813.

16. Vamvatsikos D, Cornell CA. Direct estimation of the seismic demand and capacity of MDOF systems through incremental dynamic analysis of an SDOF approximation. *J Struct Eng*. 2005;131(4):589-599.
17. O'Reilly GJ, Sullivan TJ. Quantification of modelling uncertainty in existing Italian RC frames. *Earthquake Eng Struct Dyn*. 2018;47(4):1054-1074.
18. Shahnazaryan D, O'Reilly GJ, Monteiro R, IPBSD 2021. https://doi.org/10.5281/zenodo.5035061
19. CEN. *EC. EN 1992-1-1 Eurocode 2: Design of Concrete Structures – Part 1-1: General Ruels and Rules for Buildings. Brussels*. European Committee for Standardization (CEN); 2004.
20. Bentz E, Appendix A : Program Manuals from Sectional Analysis of Reinforced Concrete Members By: Graduate Department of Civil Engineering University of Toronto, 2015.
21. Haselton CB, Liel AB, Taylor-Lange SC, Deierlein GG. Calibration of model to simulate response of reinforced concrete beam-columns to collapse. *ACI Struct J*. 2016;113(6):1141-1152.
22. McKenna F, Scott MH, Fenves GL. Nonlinear finite-element analysis software architecture using object composition. *J Comput Civil Eng*. 2010;24(1):95-107.
23. Hall JF. Performance of viscous damping in inelastic seismic analysis of moment-frame buildings. *Earthquake Eng Struct Dyn*. 2018;47(14):2756-2776.
24. Cosenza E, Del Vecchio C, Di Ludovico M, et al. *The Italian Guidelines for Seismic Risk Classification of Constructions: Technical Principles and Validation*. Springer Netherlands; 2018. https://doi.org/10.1007/s10518-018-0431-8.
25. Ramirez CM, Liel AB, Mitrani-Reiser J, et al. Expected earthquake damage and repair costs in reinforced concrete frame buildings. *Earthquake Eng Struct Dyn*. 2012;41(11):1455-1475.
26. Goulet CA, Haselton CB, Mitrani-reiser J, et al. Evaluation of the seismic performance of a code-conforming reinforced-concrete frame building—from seismic hazard to collapse safety and economic losses 2007 (June): 1973-1997. https://doi.org/10.1002/eqe
27. Duckett W, Risk Analysis and the Acceptable Probability of Failure 2004(July): 1-5.
28. Fajfar P, Dolšek M, A practice - oriented estimation of the failure probability of building structures 2012(July 2011):531-547. https://doi.org/10.1002/eqe
29. Dolšek M, Lazar Sinković N, Žižmond J. IM-based and EDP-based decision models for the verification of the seismic collapse safety of buildings. *Earthquake Eng Struct Dyn*. 2017;46(15):2665-2682.
30. Silva V, Crowley H, Bazzurro P. Exploring risk-targeted hazard maps for Europe. *Earthquake Spectra*. 2016;32(2):1165-1186.
31. Ibarra LF, Medina RA, Krawinkler H. Hysteretic models that incorporate strength and stiffness deterioration. *Earthquake Eng Struct Dyn*. 2005;34(12):1489-1511.
32. Pagani M, Monelli D, Weatherill G, et al. OpenQuake Engine : an Open Hazard (and Risk) Software for the Global Earthquake Model 2014 (September). https://doi.org/10.1785/0220130087
33. Woessner J, Wiemer S. Assessing the quality of earthquake catalogues: estimating the magnitude of completeness and its uncertainty. *Bull Seismol Soc Am*. 2005;95(2):684-698.
34. Ancheta TD, Darragh RB, Stewart JP, et al. NGA-West2 database. *Earthquake Spectra*. 2014;30(3):989-1005.
35. Shahnazaryan D, O'Reilly GJ, Monteiro R, Using direct economic losses and collapse risk for seismic design of RC buildings. COMPDYN Proceedings, vol. 3, 2019.
36. Di Ludovico M, Prota A, Moroni C, Manfredi G, Dolce M. Reconstruction process of damaged residential buildings outside historical centres after the L'Aquila earthquake: part I—"light damage" reconstruction. *Bull Earthquake Eng*. 2017;15(2):667-692.
37. FEMA. *FEMA P58-3. Seismic Performance Assessment of Buildings Volume 3 – Performance Assessment Calculation Tool (PACT)*.: 2012.
38. Cardone D. Fragility curves and loss functions for RC structural components with smooth rebars. *Earthquake Struct*. 2016;10(5):1181-1212.
39. Cardone D, Perrone G. Developing fragility curves and loss functions for masonry infill walls. *Earthquake Struct*. 2015;9(1):257-279.
40. Sassun K, Sullivan TJ, Morandi P, Cardone D. Characterising the in-plane seismic performance of infill masonry. *Bull N Z Soc Earthquake Eng*. 2016;49(1):98-115.
41. Silva A, Castro JM, Monteiro R. A rational approach to the conversion of FEMA P-58 seismic repair costs to Europe. *Earthquake Spectra*. 2020;36(3):1607-1618.
42. De Risi MT, Del Gaudio C, Verderame GM. *A Component-Level Methodology to Evaluate the Seismic Repair Costs of Infills and Services for Italian RC Buildings*. Springer Netherlands; 2020. https://doi.org/10.1007/s10518-020-00944-7.
43. Ramirez CM, Miranda E. Significance of residual drifts in building earthquake loss estimation. *Earthquake Eng Struct Dyn*. 2012;41(11):1477-1493.
44. Calvi PM, Sullivan TJ. Estimating floor spectra in multiple degree of freedom systems. *Earthquake Struct*. 2014;7(1):17-38.
45. Welch DP, Sullivan TJ, Illustrating a new possibility for the estimation of floor spectra in nonlinear multi-degree of freedom systems. *Proceedings of the 16th World Conference on Earthquake Engineering (16WCEE), Santiago, Chile* 2017.

How to cite this article: Shahnazaryan D, O'Reilly GJ, Monteiro R. On the seismic loss estimation of integrated performance-based designed buildings. *Earthquake Engng Struct Dyn*. 2022;1–25. https://doi.org/10.1002/eqe.3638